Angular-resolved autoionization study of CO on Ni(110): Experiment and theory

T. Porwol, G. Dömötör, I. Hemmerich, J. Klinkmann, and H.-J. Freund
Lehrstuhl für Physikalische Chemie 1, Ruhr-Universität Bochum, Universitätsstrasse 150, 44780 Bochum, Federal Republic of Germany

C.-M. Liegener
Institut für Physikalische und Theoretische Chemie, Universität Erlangen-Nürnberg, Egerlandstrasse 3, 91058 Erlangen, Federal Republic of Germany

(Received 14 October 1992; revised manuscript received 18 October 1993)

Angular-resolved autoionization spectra after core-to-bound excitation of CO absorbed on Ni(110) in the $(2\times1)p2mg$ structure are presented. The experimental autoionization spectra are compared with calculated spectra for the model system Ni-CO by application of the many-body Green's-function technique using self-consistent-field results–molecular orbital–complete neglect of differential overlap one-particle wave functions. In order to supplement the semiempirical approach we furthermore carried out *ab initio* calculations of the autoionization rates. The angular dependences of the autoionization lines are explicitly calculated. The core-valence-valence Auger spectrum of Ni-CO after C_{1s} and O_{1s} excitation has been calculated by the particle-particle Green's-function method with subsequent calculation of the radiationless Auger rates. The combination of the theoretical approaches and the information gained from the angular electron distribution allows one to assign the spectra obtained after core-to-bound and core-to-continuum excitation within the framework of molecular-orbital theory.

I. INTRODUCTION

The chemisorption of carbon monoxide has been subject to many different kinds of surface spectroscopic studies and various theoretical approaches.[1–3] A particular extensively used technique is photoelectron spectroscopy.

Photoionization is a complex dynamical many-particle process. One cannot directly observe the binding energy by removing a single electron from a molecular system. This hypothetical state would only be observed if the final-state orbital wave functions are equivalent to the initial-state wave functions. The energy of this artificial state is called the Koopmans energy.[4] The deviation from this hypothetical state depends on how much the system relaxes as a function of removal of an electron.

Relaxation is experimentally obvious in high-photon-energy core-excited spectra where each line is accompanied by a rich satellite structure.[5] The experimental observation of the shakeup states in the inner valence region of molecular adsorbates is difficult, however, due to the fact that emission of secondary electrons swamps the relatively low intensity of the satellites.[6] A way out is the application of autoionization spectroscopy. In recent work, several groups have studied the autoionization spectra of gas-phase molecules, molecular solids,[7–31] and adsorbates on solid surfaces.[10,25,26,32–42] In the present work, we consider theoretical and experimental investigations on chemisorbed molecules,[10,25,26,32–42] including the option of using the angular dependence of autoionization intensities, as has been done previously for Auger spectra.[43,44]

Briefly, as shown in Fig. 1, excitation of a core electron to a bound state leads to a highly excited neutral state that decays via autoionization into valence ion states of the adsorbate. Whereas photoionization and the core-to-bound excitation are governed by dipole selection rules, the radiationless decay intensity is determined by the Coulomb operator matrix elements. The final states in autoionization of a bound-state resonance can also be reached by direct photoemission. However, due to the nature of the radiationless decay process, satellite states,

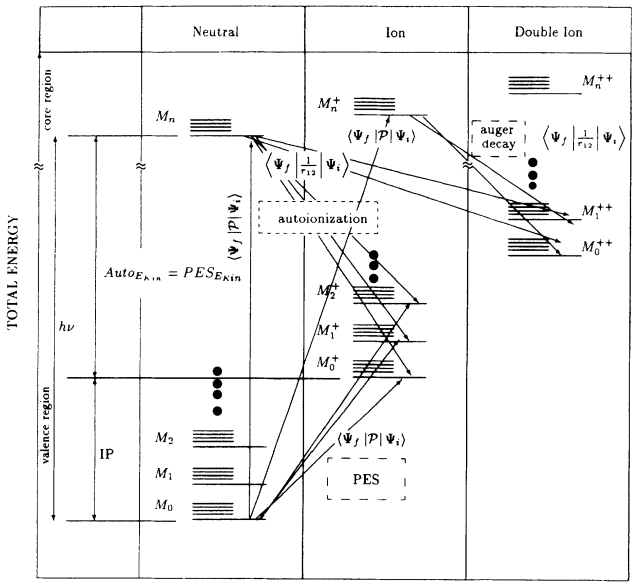

FIG. 1. Total-energy diagram of ground, valence-excited, and core-excited states of the neutral N electron (M_i), singly ionized $N-1$ electron (M_i^+), and the double ionized $N-2$ electron system (M_i^{++}). Excitations and decay channels are indicated by arrows.

which are primarily two-hole one-particle states, are populated with relatively high probability in contrast to photoemission, where one-particle hole states often dominate. Satellites that are due to two-particle hole states play, as alluded to above, an important role in the inner valence electron regime,[45,46] and, therefore, autoionization spectroscopy is well suited to studying this energy region. There is a well known connection between the energy scales of photoemission and autoionization shown in the left-hand panel of Fig. 1 (see, e.g., Ref. 10).

In contrast to autoionization, the final state of the Auger decay leads to a final state with a charge of +2. Whereas Auger and autoionization decays are well separated for molecules in the gas phase, they become more similar on surfaces. This is due to the presence of screening electrons from the metal substrate. If we look at the electronic structure of the adsorbed molecule the Auger final state, which is primarily doubly charged, will be screened by the metal electrons and resembles a singly charged system. It has been assumed that screening already occurs in the initial core-to-continuum excited state.[33] In other words, the core excited state is basically the same for the core-to-bound and core-to-continuum excitation due to screening effects. This has been used as an explanation for the experimental observation that autoionization and Auger spectra have the same overall shape.[33,38] Using the classical nomenclature of electron spectroscopy, this would imply that no Auger final states should be populated in the case of core excitation of chemisorbed molecules.

In order to assign the spectra, it is important to identify and understand the wave functions involved in those ion states leading to pronounced peaks in the spectra. While the wave function is not observable, the symmetry of the ion state involved may be deduced from angular electron distribution experiments. The electron distributions are directly related to the symmetries of the states involved by the transition matrix elements and it is the goal of this paper to provide experimental data for the angular distributions as well as to compare the data with corresponding calculations on a model system. A particularly attractive option in the present case is the observation of the angular distributions after C_{1s} and O_{1s} excitation. While in both cases the same states are reached, their amplitudes are weighted by the localized core-hole excitation.

Taking linear Ni-CO as a model system, we will show in the present paper that we are able to explain the experimental findings within the framework of molecular-orbital theory. The assignment of the spectra is supported by the explicit inclusion of the angular dependences of the transition rates of the states after core-to-bound excitation. We will show that the overall shape of spectra obtained after the two excitations are compatible, in full agreement with present and previous experimental results.[10,25,26,32–42]

The paper is organized as follows. After some basic technical considerations concerning the method of calculation and the experimental conditions we present the results and their discussion in several sections. Section IV A contains some general remarks on the overall spectra and their evaluation. In Sec. IV B, a detailed comparison of measured and calculated spectra at a particular angle (normal emission) is presented, whereas the discussion of angular distributions is given in Sec. IV C. The last section, IV D, contains a brief comment on the comparison of autoionization spectra and Auger spectra.

II. THEORETICAL CONSIDERATIONS

The decay of a core excited state might proceed by autoionization or Auger processes. If we excite the system with a photon into a neutral state, this state may decay radiationless via autoionization into the lower ion states of the system. Core-to-continuum excitation of the system with a photon yields a core ionized state which might, however, decay radiationless via Auger decay to double ionized states. Within the Green's-function formalism, we calculate the autoionization as well as the Auger spectrum for the model system Ni-CO by means of complete neglect of differential overlap (CNDO) and *ab initio* wave functions.

It has been shown recently[47] that there are discrepancies between CNDO/2 and *ab initio* results. It is well known that CNDO eigenvalues are shifted to higher binding energies by 3–5 eV with respect to *ab initio* calculations. These values enter directly into the Dyson equation, resulting in relatively high binding energies for the satellite states ($2h$-$1p$). The satellite states cannot be shifted to lower binding energies because of a singularity of the real part of the self-energy. Therefore, in the present work we have used the eigenvalues obtained with a large Gaussian basis set by Ohno and von Niessen.[47] It turns out that the results of the one-particle Green's-function calculation obtained show no major discrepancies to the *ab initio* results. However, it is well known that in semiempirical Green's-function calculations, single-hole states are calculated at binding energies that are too low.[48,49] Due to the smooth behavior of the real part of the self-energy, the single-hole ($1h$) states can be shifted to higher binding energies.

In order to judge the quality of the semiempirical approach, we furthermore carried out *ab initio* calculations of the autoionization rates using the wave function of Ohno and von Niessen.[47]

A. Calculation of the autoionization spectra

The results of a Green's-function calculation on the CNDO level[50,49] have been used to describe the valence ion states of Ni-CO up to 50 eV binding energy within the limit of sudden approximation. We have used the ion-state configuration interaction (CI) eigenvectors to calculate the transition probabilities for autoionization from the neutral highly excited state (a) to the valence ionized states (b),

$$I_{ab} \propto \sum_{l,m} |\langle \Psi^b_{\text{ion}} e^{(lm)} | \hat{H} | \Psi^a_{\text{neutral}} \rangle|^2 . \quad (1)$$

Ψ^a_{neutral} represents the initial autoionizing state of the molecule, Ψ^b_{ion} is the final ion state, $\hat{H}$ and $e^{(lm)}$ are the Hamiltonian and the departing electron, respectively.

The initial-state wave function is approximated as

$$|\Psi^a_{\text{neutral}}\rangle \approx |\phi_{1s\to\pi^*}\rangle \ , \tag{2}$$

i.e., a single determinant representation was chosen for the core-to-bound excited neutral state. For the final-state wave function, a configuration-interaction representation has to be used,

$$|\Psi^b_{\text{ion}} e^{(lm)}\rangle \approx |\hat{A} \sum_{\mu} c_{\mu b} |\phi_\mu\rangle \psi_{lm} \ , \tag{3}$$

where $\hat{A}$ represents the antisymmetrizer, ψ_{lm} are spherical waves centered at the core-hole site characterized by a set of angular-momentum quantum numbers (l,m), describing the emitted electron. In Eq. (3), μ enumerates the possible final-state configurations. The ion-state CI eigenvectors have been taken from the calculation described above. Within this approximation, the intensity is given as

$$I_{ab} = \sum_{l,m} \sum_{\mu,\nu} c^*_{\mu b} c_{\nu b} \langle \hat{A}\phi_\mu \psi_{lm} | \hat{H} | \phi_i \rangle \langle \phi_i | \hat{H} | \hat{A}\phi_\nu \psi_{lm} \rangle \ . \tag{4}$$

Using the abbreviation

$$M^{lm}_\nu = \langle \phi_i | \hat{H} | \hat{A}\phi_\nu \psi_{lm} \rangle \ , \tag{5}$$

Eq. (4) reduces to

$$I_{ab} = \sum_{l,m} \sum_{\mu,\nu} c^*_{\mu b} c_{\nu b} M^{lm*}_\mu M^{lm}_\nu \ . \tag{6}$$

It has been shown elsewhere[51] that one has to differentiate four different types of valence-ionized doublet final states under the assumption that the ground state of the molecule is a $^1\Sigma$ state. Without going into detail for single-hole states, one obtains

$$M^{lm} = 2V_{1s\psi\pi^* i} - V_{1s\psi i\pi^*} \ , \tag{7}$$

with the abbreviation

$$V_{1s\psi\pi^* i} = \left\langle \phi_{1s}(1)\psi_{lm}(2) \left| \frac{1}{r_{12}} \right| \phi_{\pi^*}(1)\phi_i(2) \right\rangle \ . \tag{8}$$

For $2h$-$1p$ configurations, one has to calculate the following matrix elements M^{lm}.

(1) $2h$-$1p$ (singlet-coupled doublet): $(i<j)$

$$M^{lm} = \frac{1}{\sqrt{2}} (V_{1s\psi ij} + V_{1s\psi ji}) \ . \tag{9}$$

(2) $2h$-$1p$ (triplet-coupled doublet): $(i<j)$

$$M^{lm} = \frac{\sqrt{3}}{\sqrt{2}} (V_{1s\psi ij} + V_{1s\psi ji}) \ . \tag{10}$$

(3) $2h$-$1p$ both holes in the same spatial orbital: $(i=j)$

$$M^{lm} = V_{1s\psi ii} \ . \tag{11}$$

The molecular orbitals ϕ_k are written as a linear combination of atomic orbitals (LCAO).

$$\phi_k = \sum_s c^k_s \chi_s \quad \text{with } k = i,j \ . \tag{12}$$

Using the LCAO one can rewrite the remaining two electron integrals and evaluate them in the so-called one-center approximation proposed by Siegbahn, Asplund, and Kelfve[52]

$$J_{lm} = \left\langle \phi_i(1)\phi_j(2) \left| \frac{1}{r_{12}} \right| \phi_{1s}(1)\psi_{lm}(2) \right\rangle \ , \tag{13}$$

$$= \sum_{r,s} c^i_r c^j_s \left\langle \chi_i(1)\chi_j(2) \left| \frac{1}{r_{12}} \right| \phi_{1s}(1)\psi_{lm}(2) \right\rangle \ , \tag{14}$$

$$= \sum_{l'm'} \sum_{l''m''} c^i_{l'm'} c^j_{l''m''} \delta(m'+m'',m) \times \sum_k c^k(l'm',00) c^k(lm,l''m'') \times R^k(nl'nl'',0l) \ . \tag{15}$$

In order to study the angular dependence of the autoionization spectra, we consider the final-state wave function Ψ_F as[53]

$$\Psi_F = 4\pi \sum_{l,m} i^l \exp(i\beta_l) Y^*_{lm}(\mathbf{k}) Y_{lm}(\mathbf{r}) G_{kl}(r) \ , \tag{16}$$

where $\mathbf{k}$ is the unit vector pointing in the direction of the outgoing electron. $G_{kl}(r)$ represents the radial part of the wave function and β_l is the phase factor of the l^{th} partially scattered wave. The choice of the one-center approximation has an important consequence: The dependence of the angularly resolved autoionization current on the azimuthal angle is lost, while the dependence on the polar angle remains. Therefore, in the calculations we have assumed a linear CO metal bond. Upon comparison with experiment, the tilt angle was taken into account. In a first very crude approximation, we are using the numerically evaluated radial integrals of McGuire[54,55] again in order to calculate the matrix elements for the radiationless decay. In order to calculate the differential intensity, Eq. (6) has to be modified as follows:

$$I_{ab}(\vartheta) = \sum_{l,m} \sum_{\mu,\nu} c^*_{\mu b} c_{\nu b} M^{lm*}_\mu M^{lm}_\nu Y_{lm}(\vartheta,\varphi) Y^*_{lm}(\vartheta,\varphi) \ . \tag{17}$$

Taking configuration interaction into account, the intensity for radiationless decay is just a function of the polar angle ϑ because

$$M^{lm}_\mu M^{lm*}_\nu [Y_{lm}(\vartheta,\varphi) Y^*_{lm}(\vartheta,\varphi)] = [(C^\mu_{1lm} J^\mu_{lm} + C^\mu_{2lm} K^\mu_{lm}) Y_{lm}(\vartheta,\varphi)] \times [(C^{\nu*}_{1lm} J^{\nu*}_{lm} + C^{\nu*}_{2lm} K^{\nu*}_{lm}) Y^*_{lm}(\vartheta,\varphi)] \ , \tag{18}$$

$$= (C^\mu_{1lm} J^\mu_{lm} + C^\mu_{2lm} K^\mu_{lm})(C^{\nu*}_{1lm} J^{\nu*}_{lm} + C^{\nu*}_{2lm} K^{\nu*}_{lm}) \text{const.}(lm) [P_{lm}(\cos\vartheta)]^2 \ , \tag{19}$$

where $P_{lm}(\cos\vartheta)$ are the well known associated Legendre polynomials,[56] and $C_{1lm}^{\mu,\nu}$ and $C_{2lm}^{\mu,\nu}$ are coefficients belonging to matrix elements $J_{lm}^{\mu,\nu}$ and $K_{lm}^{\mu,\nu}$, respectively. The spherical harmonics are orthogonal for different l and m, and they are normalized so that their integrated square over the sphere is unity. Integration of the differential angular-dependent intensities over the sphere gives

$$I_{ab}=\int_0^{2\pi}\int_0^{\pi} I_{ab}(\vartheta)d\varphi d\vartheta \ , \tag{20}$$

where I_{ab} [Eq. (6)] represents the integrated intensity.

B. Calculation of the Auger spectra

In the Green's-function method employed[57–61] here, the double ionization potentials (two-hole binding energies) are obtained as (the negative of) the poles of the particle-particle Green's function. The poles are the zeros of the eigenvalues of the inverse Green's matrix given by

$$\mathcal{G}^{-1}(\omega)=\mathcal{G}^{(0)-1}(\omega)-\mathcal{H} \tag{21}$$

where $\mathcal{H}$ is the irreducible vertex part with elements specified as follows:

$$\mathcal{H}_{klmn}^{(S,T)}=V_{klmn}\pm V_{klnm} \quad \text{if } k<l \text{ and } m<n \ ,$$

$$\mathcal{H}_{klmn}^{(S)}=V_{klmn} \quad \text{if } k=l \text{ and } m=n \ ,$$

$$\mathcal{H}_{klmn}^{(S)}=\sqrt{2}V_{klmn} \quad \text{if either } k=l \text{ or } m=n \ ,$$

where V_{klmn} are the two-electron integrals and the upper/lower sign refers to singlets (S)/triplets (T), respectively. The V_{klmn} have been evaluated in the CNDO approximation here,

$$V_{klmn}=\sum_{\mu\nu} c_{k\mu}c_{l\nu}c_{m\mu}c_{n\nu}\gamma_{\mu\nu} \ , \tag{22}$$

where $c_{k\mu}$ are the orbital expansion coefficients and $\gamma_{\mu\nu}$ the Coulomb integrals in the atomic basis. Furthermore,

$$\mathcal{G}_{klmn}^{(0)}(\omega)=\sum_{i,j}\frac{F_{ki,lj}P_{ki}P_{lj}\delta_{km}\delta_{ln}}{(\omega-\omega_{ki}-\omega_{lj})} \ , \tag{23}$$

where ω_{ki} are the poles of the one-particle Green's function and P_{ki} the corresponding pole strengths (k denotes the single-ionization species and i enumerates the possible solutions for this species). The factor $F_{ki,lj}$ equals -1 if k and l belong to the set of occupied orbitals, $+1$ if k and l belong to the set of virtual orbitals, and zero otherwise.

The transition rate $W_f^{(S,T)}$ to a final state $\Psi_f^{(S,T)}$ is estimated as

$$W_f^{(S,T)}=d^{(S,T)}\sum_{l,m}\sum_{iji'j'} M_{ij}^{(S,T)}(\psi_{lm})^{*}M_{i'j'}^{(S,T)}(\psi_{lm}) \times\omega_f^{\mathrm{Res}}(-\mathcal{G}_{iji'j'}^{(S,T)}) \ , \tag{24}$$

where $d^{(S)}1, d^{(T)}=3$ and $M_{i,j}^{(S,T)}$ is the matrix element of the electronic Hamiltonian between Hartree-Fock states where the initial state has a core hole and the final state has holes in orbitals ϕ_i, ϕ_j and an additional electron in a continuum orbital which is approximated by a spherical wave function ψ_{lm}, centered at the primary ionization site. The matrix elements are evaluated in the one-center model[52] [Eq. (15)] employing the radial integrals of McGuire.[54,55]

III. EXPERIMENTAL PROCEDURE

The experiments were performed in three different magnetically shielded ultrahigh-vacuum systems containing facilities for low-energy electron diffraction (LEED), Auger electron spectroscopy (AES), residual-gas analysis with a quadrupole mass spectrometer, and angular-resolved photoelectron spectroscopy. Two of the UHV systems have been equipped with an electron analyzer which is rotatable in two orthogonal planes and electrons are collected within an acceptance angle of $\pm 1.5°$. The resolution in energy was typically 1 eV. Excitation of photoelectrons was achieved by synchrotron radiation from the exit slit of a high-energy toroidal grating monochromator[62] or a SX700 monochromator attached to the storage ring Berliner Elektronenspeicherring-Gesellschaft für Synchrotronstrahlung m.b.H. (BESSY) I in Berlin. The base pressure in the system was below 10^{-8} Pa. The Ni(110) crystal was spot welded to two tungsten rods mounted on a sample manipulator. With liquid nitrogen the crystal could be cooled to 85 K. Heating was possible either directly or by electron impact onto the reversible side of the crystal. The surface was cleaned by argon-ion bombardment. After annealing, the cleanness was checked with AES or x-ray photoelectron spectroscopy. The surface order and geometry was established by LEED.[63]

Adsorption of CO at temperatures below 200 K results at saturation in a well ordered $(2\times1)p2mg$ structure corresponding to a coverage $\Theta=1$.

The analysis of the fine structure and the angular dependence of the spectra is discussed in the Appendix.

IV. RESULTS AND DISCUSSION

A. General remarks

Figure 2 shows a set of spectra of the system $CO(2\times1)p2mg/Ni(110)$ including photoelectron, autoionization, and Auger spectra. For comparison, the photoelectron spectrum of the clean substrate is also included. It should be mentioned that the spectrum of the clean substrate does not change significantly if the photon energy is varied from 250 to 550 eV. Figure 2 shows two photoelectron spectra of the adsorbate, one at 278 eV, where the adsorbate-induced features at 8 and 11 eV are very weak, and a spectrum taken at 35.4 eV to clearly reveal the positions of these features. The observed splittings in the adsorbate levels are due to the nonsymorphic space group of the system and are well understood.[64,65] In the photoelectron spectra taken with 278-eV photon energy, there is hardly any adsorbate-induced intensity found above 15 eV binding energy because the secondary electrons from the metallic substrate create an intense background. A way out is to tune the photon energy into the so-called Cooper minimum of the transition-metal cross section, which has recently been demonstrated by Mårtensson and his group.[25,66,67] However, first-row transition metals exhibit no Cooper minima. Here it is

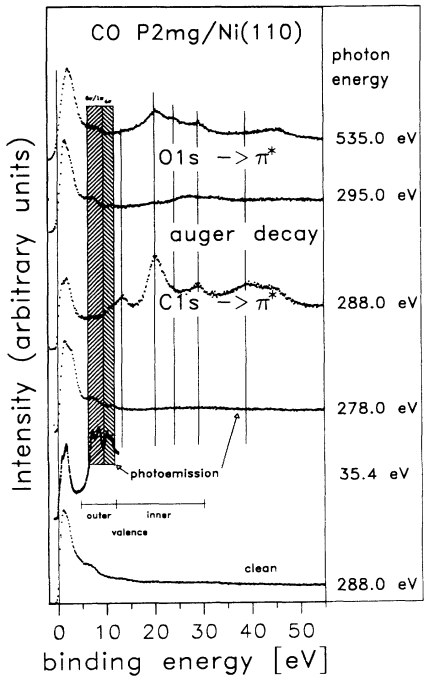

FIG. 2. Series of photoelectron spectra, autoionization spectra, and an Auger spectrum taken in normal electron emission at various photon energies.

possible to use photon energies close to 100 eV, where the electron escape depth is minimized, although even in this case the background is still a problem. As pointed out in the Introduction, a way out is to tune the photon energy to a core-to-bound transition and record the electron spectrum due to the radiationless decay. The two traces in Fig. 2 recorded at 288 and 535 eV photon energy refer to the autoionization decay of the $C_{1s} \rightarrow 2\pi$ and the $O_{1s} \rightarrow 2\pi$ resonances, respectively. If an energy is chosen between the two autoionization resonances (shown in Fig. 2) or above the O_{1s} K edge (not shown), the normal Auger spectra are recorded. As alluded to in the Introduction, autoionization and photoionization may be put on the same binding-energy scale. Therefore, we can directly compare peak positions and intensities. Clearly, the energy regime where the photoelectron spectra reveal the well known $5\sigma/1\pi$ and 4σ adsorbate features exhibits only very weak intensities in the autoionization spectra. The opposite is true in the energy region of the so-called inner valence ionizations below 20 eV binding energy relative to the Fermi level, which exhibits very intense spectral features in autoionization. It will be the main goal of the present paper to find a consistent assignment of all spectral features in both spectroscopies. From the experimental side, we shall study the angular dependence of relative intensities of the autoionization transitions for both $C_{1s} \rightarrow \pi^*$ and $O_{1s} \rightarrow \pi^*$ resonances. From the theoretical side, we shall attempt to model the autoionization decay and its angular dependence on the basis of molecular-orbital calculations, which are augmented by configuration interaction to take the high degree of many-particle character of the processes into account. The general idea is as follows. Assume the ion state populated in an autoionization experiment has Σ^+ symmetry. The neutral state of the decay is created via a $C_{1s} \rightarrow \pi^*$ excitation and thus has Π symmetry. The intensity of a transition is governed by the Coulomb operator matrix elements discussed in the theoretical section. Taking the symmetry of the Coulomb operator into account, which is Σ^+, we can now determine the symmetry of the outgoing electron wave: The direct product of the symmetries of the final ion state Γ_{ion}, operator Γ_{op}, and initial state Γ_{ini} in this case yields symmetries Π. Now the emitted electron has to be considered. The symmetry of the continuum state of the emitted electron $\Gamma_{e^{l,m}}$ is determined by the fact that the symmetry of the total direct product

$$\Gamma_{\text{ion}} \otimes \Gamma_{\text{op}} \otimes \Gamma_{\text{ini}} \otimes \Gamma_{e^{l,m}} \subset \Sigma^+$$

has to contain the totally symmetric representation Σ^+. In other words, considering the fact that the direct product of the first three terms has been determined to be Π, the wave function of the emitted electron has to transform according to the same irreducible representation, i.e., π. An emitted π wave, for example, has a node at $\vartheta = 0°$, which can be used to assign the observed angle-dependent intensities.

Figures 3 and 4 show the angular dependences of the autoionization spectra after core-to-bound excitations near the C-K edge and the O-K edge, respectively. In both cases, the polar angle has been varied along the two high-symmetry azimuths of the Ni(110) surface, i.e., the (001) and the (110) azimuths. Both sets do not indicate any pronounced dependence on the azimuth chosen. Note that the relative changes in the low-binding-energy range for the (001) azimuth are due to effects in the photoelectron spectrum underlying the autoionization spectrum. The absence of any pronounced dependence on the azimuth is consistent with the assumption that autoionization is dominated by one-center terms (see Sec. II). In order to deduce the angular dependences of the individu-

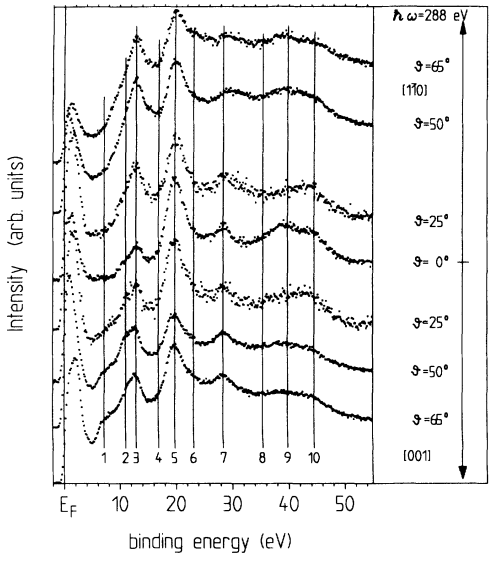

FIG. 3. Autoionization spectra after $C_{1s} \rightarrow \pi^*$ excitation taken as a function of the polar angle ϑ and with respect to the two high-symmetry azimuths [1$\bar{1}$0] and [001].

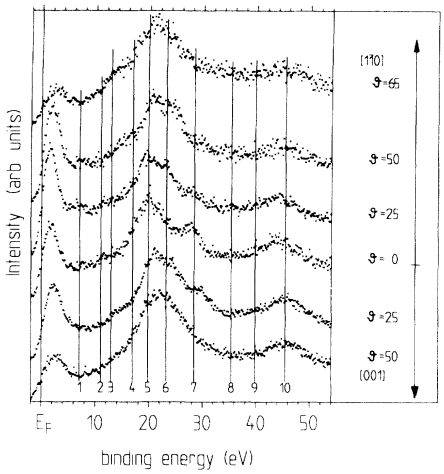

FIG. 4. Autoionization spectra after $O_{1s} \rightarrow \pi^*$ excitation taken as a function of the polar angle ϑ and with respect to the two high-symmetry azimuths [1$\bar{1}$0] and [001].

al constituent transitions of the spectrum, we have fit a set of ten student distributions to each spectrum (see positions in Figs. 3 and 4). A detailed description of the fitting procedure is given in the Appendix. The choice of ten functions is dictated by the experimental spectra because there are ten peaks or shoulders visible in the C-decay spectrum, for example. It is only peak 4 which may be debated, but this one was necessary to obtain a reasonable fit as judged by the least-squares difference. Due to the better signal-to-noise ratio, we have put more emphasis on the C-decay spectrum and carried over the number of peaks used in this case to fit the O-decay spectrum. In Figs. 5 and 6 the angular-dependent intensities are plotted for six out of the ten features (see binding energies). The functional dependence varies for the different peaks and it should be possible to use the observations to help assign a particular symmetry to the spectral feature in a similar fashion as Umbach and Hussain[43,44] deduced symmetries of Auger peaks via angular-dependent measurements. However, it is not at all obvious that each one of the ten identified features belongs to a single, well defined state of the system, thus allowing the assignment of a single unique symmetry. We have to allow from the beginning for overlap and interference between final states, which renders the problem almost hopeless without theoretical assistance.

Therefore, we have undertaken calculations of the angular-dependent autoionization cross section. These calculations are based on semiempirical or *ab initio* wave functions determined for the ion states via Green's-function calculations, which are well documented in the literature.[45,50,68–72]

B. Comparison between experiment and theory

Results of such calculations are shown in Fig. 7 in comparison with experimental data. The theoretical results had to be shifted by a constant energy increment, i.e., the work function of 5.95 eV (4.65 eV [Ni(110) clean[73]]+1.3 eV [CO-induced shift[74]]). *Ab initio* results have only been obtained up to binding energies around 20 eV. Figure 7 is arranged in two panels. The left-hand panel shows the autoionization probabilities after $C_{1s} \rightarrow \pi^*$ excitation, the right-hand panel after $O_{1s} \rightarrow \pi^*$ excitation. The following discussion must be divided into several sections, one in which the nature of the states with largest autoionization amplitudes is explained, and a second one where the results of the numerical calculations are condensed in such a way that the results can be compared with experiment in the third part. Since we are using the configuration interactions involved, it is important to realize which configurations contribute most significantly to the autoionization intensity. Table I contains the important information including the dependence of the intensities on localization of the wave function. The latter aspect has already been discussed in detail elsewhere and we do not want to repeat the arguments at this point except to note that hole localization on the carbon as well as on the oxygen is achieved via the so-called equivalent core approximation, which is well documented in the literature. The table includes two-hole-particle configurations as well as single-hole

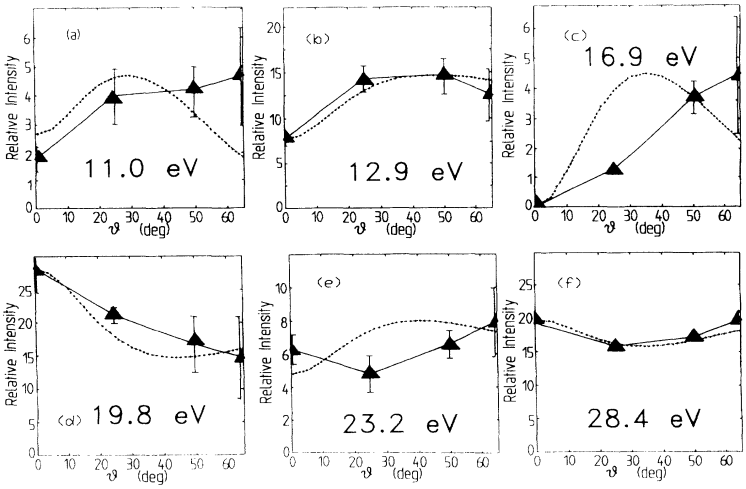

FIG. 5. Relative intensities of the spectral features centered at the given binding energies (compare Fig. 3) of the $C_{1s} \rightarrow \pi^*$ decay spectra as a function of polar angle ϑ.

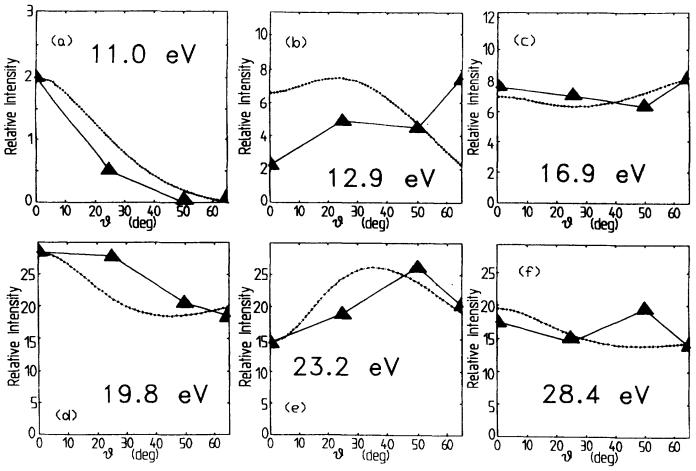

FIG. 6. Relative intensities of the spectral features centered at the given binding energies (compare Fig. 4) of the $O_{1s} \rightarrow \pi^*$ decay spectra as a function of polar angle ϑ.

configurations. As stated above, the dominant intensities are not due to the single-hole states but, rather, to the two-hole–one-particle states. There are only a few rather large ones. They may be classified as the coupling of a $1\pi \rightarrow \pi^*$ electron-hole-pair excitation to the 5σ, 1π, and 4σ holes. Note that π^* refers to the $2\pi^*$ level of CO, while 2π refers to the occupied-metal-derived π level. The other much less intense class of configurations involves the same hole states but a $2\pi \rightarrow \pi^*$ electron-hole pair, which is equivalent to a charge-transfer excitation from the metal orbital (2π) to the unoccupied CO π^* level; in other words, a screened hole state. We mark configurations with the label CT in addition to the involved hole state if the created electron-hole pair leads to a charge transfer. Their autoionization amplitudes are comparable to those of the single-hole configurations. The single-hole-state configurations may have Σ and Π symmetry. The two-hole-particle states may give size to Σ, Π, and Δ symmetries. It is one of the problems that renders the assignment problem difficult, that all states of the same symmetry are strongly mixed. In other words, the calculated spectroscopic states cannot be assigned to a particular configuration. For our present discussion, we shall group the calculated states according to the energy regions found experimentally and assign the dominant character, as revealed by the calculations, to these areas. Such an assignment is compiled in Table II. This assignment is valid for autoionization following both $C_{1s} \rightarrow \pi^*$ and $O_{1s} \rightarrow \pi^*$ excitation. If the reader is interested in the details of the calculations as far as contributions to the CI vector are concerned, Ref. 51 contains the relevant information. However, absolute and relative intensities vary considerably for both excitations because decay after $O_{1s} \rightarrow \pi^*$ excitation emphasizes different components of the wave functions in the energy range as compared with decay after $C_{1s} \rightarrow \pi^*$ excitations, as will be discussed later in this paper. Primarily, we note that the absolute $O_{1s} \rightarrow \pi^*$ decay intensities are calculated to be less intense as compared with the $C_{1s} \rightarrow \pi^*$ decay by

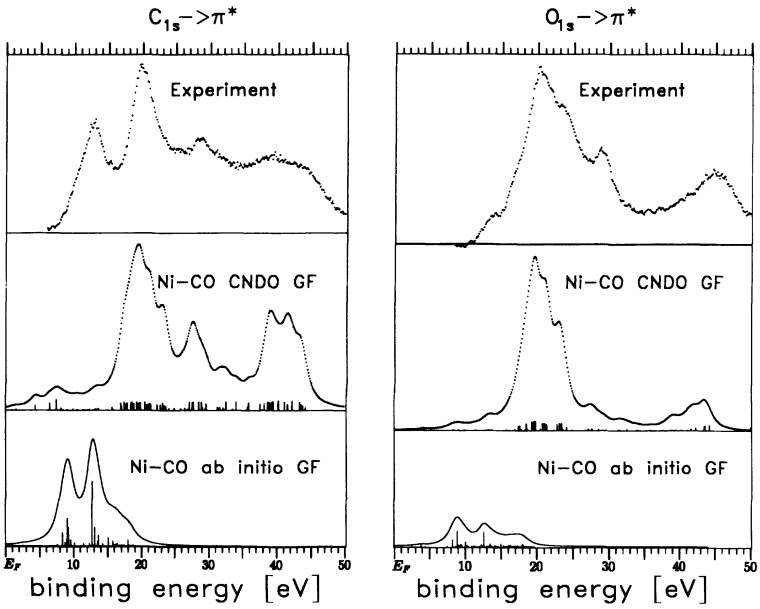

FIG. 7. Comparison between calculated and measured autoionization spectra. The calculated line spectra have been convoluted with a Lorentzian line of 2 eV full width at half maximum.

TABLE I. Autoionization matrix elements for pure configurations. The superscripts 1 and 3 indicate singlet and triplet coupled doublet final states, respectively. $2h$-$1p$ configurations without a superscript are singlet coupled doublet final states where both holes reside in the same spatial orbital.

Configuration of the final state	Wave function $O_{1s}\rightarrow\pi^*$ Ni-CO	$O_{1s}\rightarrow\pi^*$ Ni-CF$^+$	$C_{1s}\rightarrow\pi^*$ Ni-CO	$C_{1s}\rightarrow\pi^*$ Ni-NO$^+$
$(3\sigma^{-1}2\pi^{-1}\pi^*)^3$	0.006	0.006	0.000	0.002
$(4\sigma^{-1}1\pi^{-1}\pi^*)^1$	0.320	0.533	0.074	0.146
$(4\sigma^{-1}1\pi^{-1}\pi^*)^3$	0.016	0.013	0.019	0.031
$(4\sigma^{-1}2\pi^{-1}\pi^*)$	0.032	0.037	0.003	0.018
$(1\pi^{-1}1\pi^{-1}\pi^*)$	0.346	0.536	0.074	0.121
$(1\pi^{-1}1\pi^{-1}\pi^*)^1$	0.434	0.673	0.092	0.151
$(1\pi^{-1}1\pi^{-1}\pi^*)^3$	0.000	0.000	0.000	0.000
$(1\pi^{-1}5\sigma^{-1}\pi^*)^1$	0.207	0.135	0.141	0.159
$(1\pi^{-1}5\sigma^{-1}\pi^*)^3$	0.002	0.000	0.008	0.003
$(1\pi^{-1}2\pi^{-1}\pi^*)^1$	0.069	0.073	0.007	0.029
$(1\pi^{-1}2\pi^{-1}\pi^*)^3$	0.000	0.000	0.000	0.000
$(5\sigma^{-1}2\pi^{-1}\pi^*)^1$	0.021	0.009	0.006	0.019
$(5\sigma^{-1}2\pi^{-1}\pi^*)^3$	0.000	0.000	0.000	0.000
$(2\pi^{-1}2\pi^{-1}\pi^*)$	0.003	0.003	0.000	0.002
$(2\pi^{-1}2\pi^{-1}\pi^*)^1$	0.004	0.003	0.000	0.002
$(2\pi^{-1}6\sigma^{-1}\pi^*)^3$	0.000	0.000	0.000	0.000
$4\sigma^{-1}$	0.095	0.045	0.281	0.310
$1\pi^{-1}$	0.086	0.074	0.100	0.105
$5\sigma^{-1}$	0.045	0.009	0.235	0.132
$2\pi^{-1}$	0.009	0.005	0.005	0.013
$6\sigma^{-1}$	0.001	0.001	0.009	0.017

roughly a factor of 2–3. In addition, however, and more importantly, intensities of particular ion configurations show characteristic variations between $C_{1s}\rightarrow\pi^*$ and $O_{1s}\rightarrow\pi^*$ decays. Let us consider the single-hole states first. For the decay of the $C_{1s}\rightarrow\pi^*$ excited state into the single-hole states, the matrix elements are larger by a factor of 4 as compared with the $O_{1s}\rightarrow\pi^*$ decay. It is clear that an important factor for the size of the matrix elements is the overlap between the π^* orbital, the valence, and the C_{1s} orbitals. Due to the high weight in the π^* orbital on the carbon atom, this overlap is considerably larger for the decay of the $C_{1s}\rightarrow\pi^*$ excited-state edge as compared with the $O_{1s}\rightarrow\pi^*$ excited state. This, of course, is also the general reason why the $C_{1s}\rightarrow\pi^*$ decay intensity is larger as compared with the $O_{1s}\rightarrow\pi^*$ decay intensity. The relative size of matrix elements for the single-hole states indicate higher intensities for the $5\sigma^{-1}$ and $4\sigma^{-1}$ hole states after $C_{1s}\rightarrow\pi^*$ excitation and higher intensities for the $1\pi^{-1}$ hole states after $O_{1s}\rightarrow\pi^*$ excitation. This is not surprising for the $5\sigma^{-1}$ and the $1\pi^{-1}$ orbitals, but even the $4\sigma^{-1}$ orbital has a rather large matrix element for $C_{1s}\rightarrow\pi^*$ decay. There are four large matrix elements for the two-hole–one-particle states. The largest matrix elements result from the configurations $1\pi^{-1}1\pi^{-1}\pi^*$. Only the $4\sigma^{-1}1\pi^{-1}\pi^*$ and the $5\sigma^{-1}1\pi^{-1}\pi^*$ configurations lead to matrix elements of comparable, or even slightly larger, magnitude in the case of $O_{1s}\rightarrow\pi^*$ and $C_{1s}\rightarrow\pi^*$ excitation, respectively. In other words, these configurations determine the autoionization spectrum in particular above 20 eV binding energies, where the states with considerable admixture of such configurations are located. In the energy range between 11 and 20 eV, we expect autoionization into screened hole states. Generally speaking, the states with screening character lead to rather low intense features with respect to the nonscreened CO-molecule-based excitations for the semiempirical calculations. A different situation is encountered for the *ab initio* calculations, where the results indicate rather large intensities in the energy region between 10 and 20 eV. On the other hand, the *ab initio* calculations have not been extended beyond 20 eV binding energy so that the calculated intensity in the region is too small. The higher admixture of the nonscreened CO-molecule-based excitations in the case of the *ab initio* calculations leads to a comparably higher intensity in the binding-energy region between 11 and 20 eV. However, the experimentally observed decrease of the relative intensities in the latter binding-energy regime when changing from the $C_{1s}\rightarrow\pi^*$ to the $O_{1s}\rightarrow\pi^*$ excitation is not quantitatively reproduced computationally, either by the *ab initio* or by the semiempirical calculations. It is obviously an effect which is sensitive to the configuration mixing involved. Also, one has to realize that the screening mechanism is not optimally described by a model containing a single metal atom. The latter could lead to a distortion of the wave function, which may even be small, but still change the configuration mixing considerably. Even though the intensities in this particular binding-energy regime do not fit quantitatively, our calculations, which are summarized in Table I, do allow us to assign most of the experimentally observed features and we may now compare the predicted angular dependences with the measured ones. The experimental measurements of the angular dependences are shown in Fig. 5 for the $C_{1s}\rightarrow 2\pi$ decay and in Fig. 6 for $O_{1s}\rightarrow 2\pi$ decay. Here, the results have been averaged over the two independently measured azimuths. Clearly, the angular variations are rather pronounced for some features indicated by a change in relative intensities by up to a factor of 5. Included in Figs. 5 and 6 are our theoretical predictions based on the semiempirical calculations as dotted lines. In some cases the qualitative variation is reproduced quantitatively and in other cases there is only qualitative correspondence. However, we consider the overall agreement to be remarkably good. In the following we shall discuss the variations step by step, i.e., with respect to energy range, using Table II with the given assignment and Fig. 8, where the angular dependences for particular pure configurations are plotted. Some systematics may be observed. Figure 8(b) shows angular dependences of configurations with either continuously increasing intensity towards off-normal angles or with a maximum at 45°. Figure 8(a) shows the corresponding data for configurations with maxima at 0° and a minimum at 45°. The different behavior can be understood on the basis of symmetry considerations as outlined above. The configurations in Fig. 8(b) are either of type σ^{-1} or $\sigma^{-1}\pi^{-1}\pi$. Therefore, the ion states resulting from these configurations, have either Σ^+, Σ^-, or Δ symmetry

TABLE II. Assignment of the autoionization spectra.

E_B^{auto}	Assignment	Angular dependence
7.1	$5\sigma^{-1}/1\pi^{-1}$ CT/$1\pi^{-1}$	
11.0	$4\sigma^{-1}/4\sigma^{-1}$ CT, $5\sigma^{-1}$ CT, $1\pi^{-1}$ CT	+
12.9	$4\sigma^{-1}$ CT	+
16.9	$1\pi^{-1}$ CT/$1\pi^{-1}5\sigma^{-1}\pi^*/1\pi^{-2}\pi^*$	+
19.8	$1\pi^{-1}4\sigma^{-1}\pi^*/1\pi^{-2}\pi^*$	+
23.2	$4\sigma^{-1}1\pi^{-1}\pi^*/1\pi^{-2}\pi^*$ triplet	+
28.4	$4\sigma^{-1}1\pi^{-1}\pi^*/5\sigma^{-1}1\pi^{-1}\pi^*$ triplet	+
35.4	$1\pi^{-2}\pi^*/4\sigma^{-1}5\sigma^{-1}\pi^*$ triplet	
39.8	$3\sigma^{-1}1\pi^{-1}\pi^*/3\sigma^{-1}$	
45.5	$3\sigma^{-1}1\pi^{-1}\pi^*$	

within the point group $C_{\infty v}$. According to the symmetry arguments outlined in the last section this means that the outgoing electron wave must have π or ϕ symmetry. An emitted π wave, for example has a node at $\vartheta=0°$ which is consistent with the observed angular dependent intensities in Fig. 8(b).

A similar argument applies for the angle dependent behavior in Fig. 8(a). Briefly, the ion-state symmetries for configurations of type $\pi^{-1}, \pi^{-2}\pi, \pi^{-1}\pi^{-1}\pi$ are Π and Δ. The direct product between ion states, operator, and initial state transforms as Σ^+, Σ^-, Δ, and Γ. Thus, the initial emitted electrons wave function transform accordingly, i.e., σ^+, σ^-, δ or γ. An emitted σ wave, as an example, has nonvanishing intensities at $\vartheta=0°$ in accord with the results in Fig. 8(a). We would find similar angular dependences for states containing configurations of type $\sigma^{-1}\sigma^{-1}\pi$. To compare with our experiments the tilting of the molecule has to be considered [i.e., 17° (Ref. 64)]. Such a tilt would lead to a shift by 17° to the left in the angle scale of Fig. 8. Note, however, that the *p2mg* structure contains two CO molecules tilted in opposite directions.

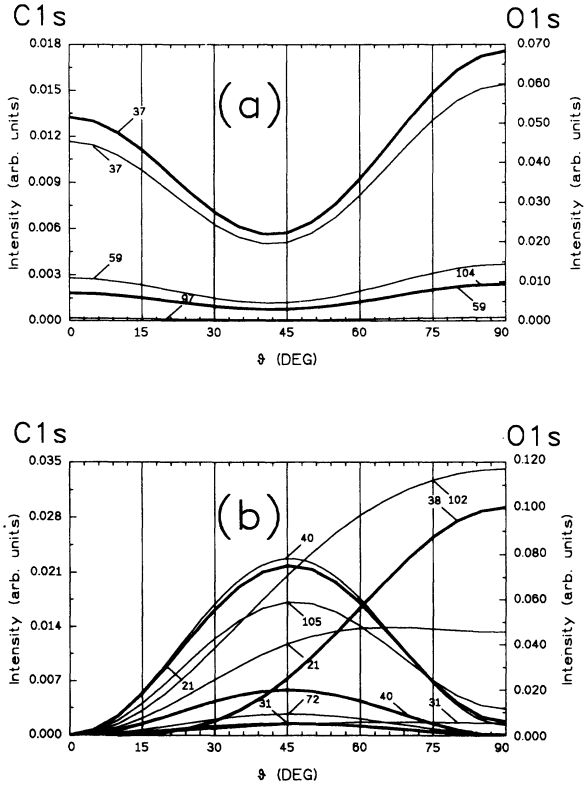

FIG. 8. Calculated angular dependences of autoionization intensities of pure configurations for CO oriented perpendicular to the surface plane. $C_{1s}\rightarrow\pi^*$ decay refers to the left-hand side intensity scale (thin lines), $O_{1s}\rightarrow\pi^*$ decay refers to the right-hand side intensity scale (thick lines). (a) $37\equiv 1\pi^{-2}\pi^*$, $59\equiv(1\pi^{-1}2\pi^{-1}\pi^*)^1$, $97\equiv 2\pi^{-2}\pi^*$, $104\equiv 1\pi^{-1}$. (b) $102\equiv 4\sigma^{-1}$, $38\equiv(1\pi^{-1}1\pi^{-1}\pi^*)^1$, $40\equiv(1\pi^{-1}5\sigma^{-1}\pi^*)^1$, $105\equiv 5\sigma^{-1}$, $21\equiv(1\pi^{-1}4\sigma^{-1}\pi^*)^1$, $31\equiv(4\sigma^{-1}2\pi^{-1}\pi^*)^1$, $72\equiv(5\sigma^{-1}2\pi^{-1}\pi^*)^1$.

C. Angular dependences

Let us now discuss the angular dependences of the autoionization spectrum directly in comparison with the calculations for six energy regions.

1. Energy range centered at 11.0 eV binding energy

Experimentally, the intensity after $C_{1s}\rightarrow\pi^*$ excitation increases from a finite value at $\vartheta=0°$ by about a factor of 2 towards $\vartheta=65°$. For the $O_{1s}\rightarrow\pi^*$ excitation we observe the reverse behavior, namely, a decrease from $\vartheta=0°$ to noise level at $\vartheta=50°$. Even though our theoretical results fail, in the case of the decay at the carbon edge, to quantitatively reproduce the behavior for larger angles, the observed differences between the two edges may be qualitatively understood on the basis of our theoretical results. The main contributions to the states around 11 eV are the $5\sigma^{-1}$, $1\pi^{-1}$, and $4\sigma^{-1}$ CT configurations, as well as the $4\sigma^{-1}$ single-hole states (see Table II). Upon excitation at the carbon edge, the autoionization is dominated (Table I) by the $5\sigma^{-1}$ and $4\sigma^{-1}$ CT configuration, which leads to an intensity increase towards larger angles [see configurations 31 and 72 in Fig. 8(b)]. However, at the oxygen edge the autoionization into a $1\pi^{-1}$ CT clearly dominates and thus the angular dependence leads to a decrease towards higher angles [see configuration 59 in Fig. 8(a)].

2. Energy range centered at 12.9 eV binding energy

Experimentally, the intensity after $C_{1s} \rightarrow \pi^*$ excitation increases from a finite value at $\vartheta = 0°$. Around $\vartheta = 45°$ the intensity does not increase any more. This is very well reproduced by the calculations, indicating that the assignment towards a 4σ-CT configuration is basically correct. The $O_{1s} - .\pi^*$ decay data are rather similar in this case except for the largest angles, where the $O_{1s} \rightarrow \pi^*$ experiments seem to indicate a further increase in intensity. The calculations fail to reproduce this latter effect and it is not clear what causes this. It should be pointed out, however, that this energy range is situated in the slope of a very intense peak, and that in this case, given the poorer signal-to-noise ratio for the $O_{1s} \rightarrow \pi^*$ decay, the fitting procedure leads to rather large error bars in the intensities. In this respect the assignment is consistent with experiment.

3. Energy range centered at 16.9 eV binding energy

Experimentally, angular variations after $C_{1s} \rightarrow \pi^*$ and $O_{1s} \rightarrow \pi^*$ decay are very dissimilar. After $C_{1s} \rightarrow \pi^*$ decay the intensity strongly increases off-normal, while after $O_{1s} \rightarrow \pi^*$ decay the intensity is almost constant as a function of angle. Both effects are qualitatively reproduced by the calculations. The reason for this behavior is that after $C_{1s} \rightarrow \pi^*$ decay the $5\sigma^{-1}1\pi^{-1}\pi^*$ configuration dominates, which leads to the increase towards higher angles, while after $O_{1s} \rightarrow \pi^*$ decay the $1\pi^{-2}\pi^*$ configuration, which has large matrix elements in this case, counteracts and renders the intensity almost independent of angle.

4. Energy range centered at 19.8 eV binding energy

Both experimentally observed angular variations indicate decreasing intensity for off-normal emission, which is also reproduced by the calculations. This indicates that in both cases the $1\pi^{-2}\pi^*$ configuration dominates the probability of the autoionization decay. It appears that the most intense feature in both the $C_{1s} \rightarrow \pi^*$ and $O_{1s} \rightarrow \pi^*$ decay spectra correlates with states originating mainly from the $1\pi^{-2}\pi^*$ configuration, showing that in particular for the $O_{1s} \rightarrow \pi^*$ decay, this configuration, where all electrons involved in the process are in the π space of the system, is the most important one. Intuitively this appears reasonable because the electron excited in the primary process resides in π space so that the Coulomb correlation, which triggers radiationless decay, is maximized.

5. Energy range centered at 23.2 eV binding energy

The angular dependence after $C_{1s} \rightarrow \pi^*$ decay is very weak, while after $O_{1s} \rightarrow \pi^*$ decay we find a slight increase of intensities towards off-normal angles. The configurations contributing predominantly to this energy range are of $4\sigma^{-1}1\pi^{-1}\pi^*$ and $1\pi^{-2}\pi^*$ types. They compensate their opposing angular variations to yield rather small overall effects. The observation that after $O_{1s} \rightarrow \pi^*$ decay the intensity increases to off-normal angles seems to indicate a large contribution from the $1\pi^{-2}\pi^*$ configurations where the two holes are located in the two perpendicular components of the 1π orbital. It would be best described as a $1\pi^{-1}1\pi^{-1}\pi^*$ configuration.

6. Energy range centered at 28.4 eV binding energy

The situation is rather similar to the last case (5) indicating that this peak originates from the same configurations that contribute to a series of ion states located at different energies in the autoionization spectra.

Summarizing, the comparison between experimentally observed angular variation of the relative autoionization probability and the computationally predicted angular dependences on the basis of our semiempirical and *ab initio* calculations shows qualitatively satisfactory agreement. It seems that the assignment given by the calculations allows us to understand the experimental observations although the agreement between computations and experiment is far from being quantitative. It would be highly desirable to perform full *ab initio* calculations with larger cluster models in order to get even deeper insight into the problem.

It is now appropriate to comment on the autoionization spectrum of free CO.[24] The $C_{1s} \rightarrow \pi^*$ decay spectrum is characterized by two most intense features between 20 and 30 eV. This corresponds to approximately 15 and 25 eV binding energy with respect to the Fermi energy. These features are due to configurations of types $5\sigma^{-2}\pi^*$, $5\sigma^{-1}4\sigma^{-1}\pi^*$, and $5\sigma^{-1}1\pi^{-1}\pi^*$.[17,24] Configurations of type $1\pi^{-2}\pi^*$ do not play a dominant role. It is clear from the above discussion of the autoionization spectrum of the adsorbate that this is a difference between the adsorbate and the gas phase. The reason must be the delocalization of the 5σ and 2π orbitals into the metal substrate which leads to rather small matrix elements especially for those configurations where the 5σ orbital is involved.

D. Comparison between autoionization and Auger decay

As alluded to in the Introduction, the comparison of autoionization and Auger spectra of adsorbates has been extensively discussed.[10,11,14,21,22,33–37,39–41,51] Due to screening of the core ionized state before Auger decay, the core ionized-state wave function of the adsorbed CO molecule looks like a core-to-bound excited state where the excited electron has been transferred from metal. We can test this idea on the basis of our model calculations. Figure 9 shows a comparison of the theoretically calculated C-KVV Auger spectrum and the above-discussed autoionization spectrum of the C_{1s} edge of the model Ni-CO cluster. A detailed analysis, especially of the angular effects in the Auger spectrum, will be published elsewhere. Here we only want to mention the general trends important for the comparison. There is a one-to-one correspondence in the features of the two spectra if the peak at lowest kinetic energy is aligned with the lowest binding-energy peak in the autoionization spectrum. The assignment of the peaks obviously is very similar as far as

the contribution of configurations to the main peaks is concerned. For the Auger spectra a $1\pi^{-2}$ configuration is equivalent to a $1\pi^{-2}\pi^*$ configuration in the autoionization spectrum because the screening electron (π^*) in the Auger case is not counted. However, the Auger and autoionization spectra, at least in the case of the Ni-CO cluster model, are not identical as far as relative intensities are concerned because the initial wave functions as well as the final states are not completely identical. The general appearance of the spectra is very similar, which corroborates some of the arguments discussed in the literature. We do not know at present whether larger metal clusters will alter the theoretical result and render the two sets of spectra indistinguishable.

In order to allow comparison with assignments put forward in the literature, we refer to Table III. With the exception of the results of Jennison *et al.*[30] for carbonyl compounds where the authors support their assignment by theoretical calculations, the assignments presented in Table III are exclusively based on experimental data. First, it is noted that previous assignments were rather selective, i.e., only very few bands were treated. In his thesis, Wurth[33] presented the most complete assignment so far. As is obvious from Table III, the present assignment is compatible with the literature assignment, the only exception being the first state in the last column of Table III. The reason for this discrepancy is not clear at present. A detailed analysis of the assignment by Ohno

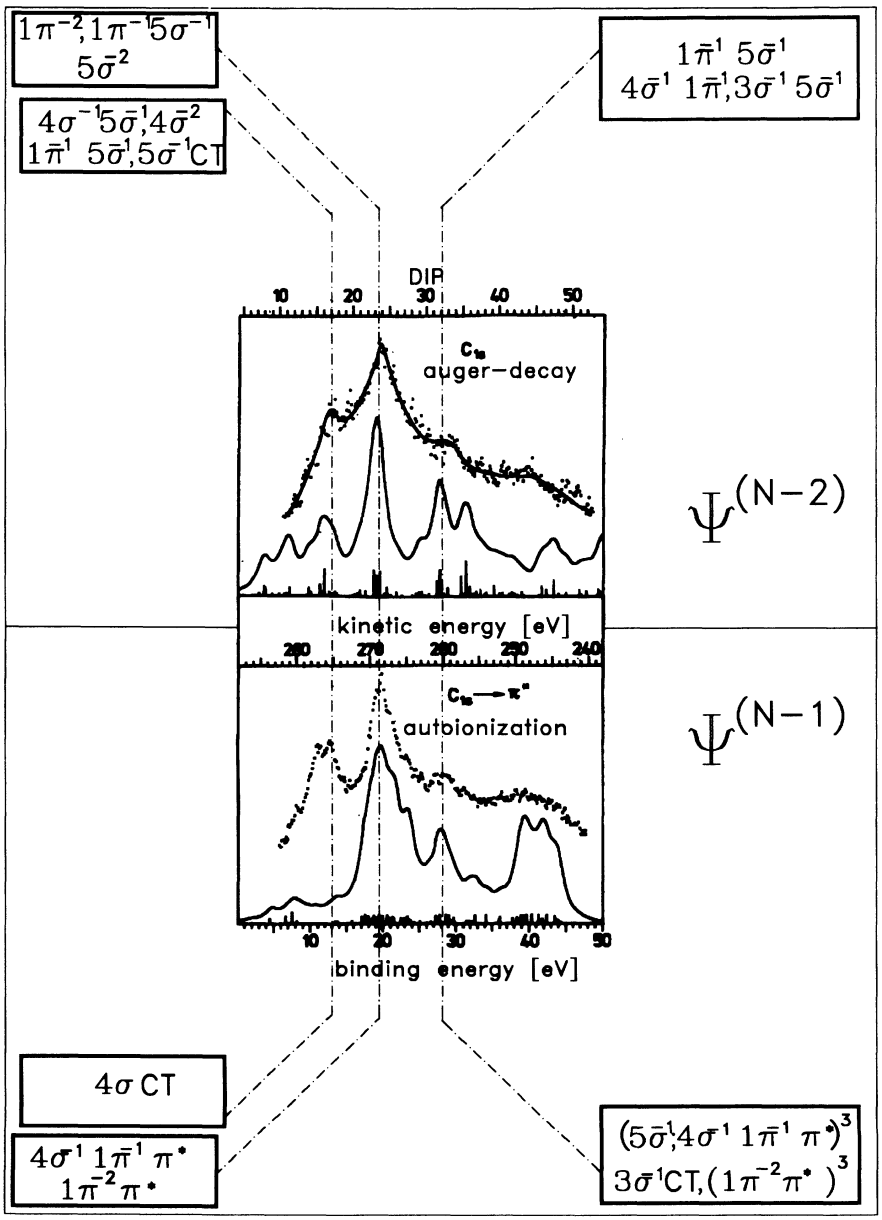

FIG. 9. Comparison of $C_{1s} \rightarrow \pi^*$ autoionization and C-KVV Auger spectra (experiment is shown as dots in the case of the Auger spectrum; a line to guide the eye is included. Theory is shown as a solid line). The main contributing configurations are given for three intense features.

and von Niessen[47,37] is not possible at the moment because calculations supporting this assignment are lacking. We note, however, that the observed angular dependence is in agreement with our assignment.

V. SUMMARY AND CONCLUSIONS

The present work connects for the first time, to our knowledge, photoionization, autoionization and Auger spectra of an adsorbate, i.e., CO/Ni within a joint theoretical and experimental effort. The autoionization spectra have been recorded as a function of the polar angle, and the experimentally observed angular dependences are compared with theoretical predictions. Figure 10 shows in a self-explanatory fashion the final assignment of the autoionization decay both at the carbon and at the oxygen edge simultaneously. The observed angular variations are in line with the assignment. We point out qualitatively that the Auger spectrum is expected to be qualitatively similar to the autoionization spectrum due to screening effects, but in detail relative intensities may be slightly different. A comparison with a corresponding set of calculations of the free CO molecule indicates that the Auger and autoionization decay in the adsorbate is completely different from the gas phase. In fact, the involvement of configurations involving the 5σ orbital of CO, which is important in the gas phase, is completely lost upon adsorption probably due to the 5σ participation in the interaction with the metal. Instead, configurations involving the 1π orbital, become very important not only for the autoionization decay but also for the Auger decay.

ACKNOWLEDGMENTS

The assistance of M. Neuber, M. Neumann, and D. R. Batchelor is gratefully acknowledged. We would like to thank K. von Niessen for providing us with the *ab initio* wave function of Ni-CO in machine-readable form. The present work was financially supported in part by the

TABLE III. Assignment of the autoionization and Auger spectra. All energies are given in eV.

E_B^{auto}	E_{kin}[a]	$C_{1s}\rightarrow\pi^*$[b]	C-KVV[b]	$C_{1s}\rightarrow\pi^*$[c]	$C_{1s}\rightarrow\pi^*$[d]	$C_{1s}\rightarrow\pi^*$[e]	C-KVV[f] E_{kin}		O-KVV[g] E_{kin}		[h]
7.1		$5\sigma^{-1}$	$2\pi^{-1}6\sigma^{-1}$				268	5σ CT			
		$1\pi^{-1}$ CT	$4\sigma^{-1}2\pi^{-1}$	$1\pi^{-1}$ CT							
		$1\pi^{-1}$	$2\pi^{-2}$	$5\sigma^{-1}$ CT							
			$5\sigma^{-1}2\pi^{-1}$								
11.0		($4\sigma^{-1}$, $5\sigma^{-1}$, $1\pi^{-1}$) CT	$5\sigma^{-2}$	$4\sigma^{-1}$ CT	$5\sigma 2\pi$		262	1π CT			$2\pi^{-2}$
		$4\sigma^{-1}$	$4\sigma^{-1}1\pi^{-1}$								
			$5\sigma^{-1}2\pi^{-1}$								
12.9	274	$4\sigma^{-1}$ CT	$4\sigma^{-1}5\sigma^{-1}/4\sigma^{-2}$		$5\sigma 2\pi$	$5\sigma 2\pi$					$5\sigma^{-1}2\pi^{-1}$
			$1\pi^{-1}5\sigma^{-1}$		$1\pi 2\pi$	$1\pi 2\pi$	$1\pi 2\pi$				
			$5\sigma^{-1}$ CT	$4\sigma^{-1}$ CT							
16.9		$1\pi^{-1}$ CT	$4\sigma^{-1}2\pi^{-1}$								
		$1\pi^{-1}5\sigma^{-1}\pi^*$									
		$1\pi^{-2}\pi^*$	$1\pi^{-1}2\pi^{-1}$								
19.8	268	$1\pi^{-1}4\sigma^{-1}\pi^*$	$1\sigma^{-2}/1\pi^{-1}5\sigma^{-1}$	$1\pi^{-2}\pi^*$		$5\sigma^{-2}$	250	$5\sigma^{-1}1\pi^{-1}$	514	$1\pi^{-2}$	
		$1\pi^{-2}\pi^*$	$5\sigma^{-2}$	$5\sigma^{-1}1\pi^{-1}\pi^*$		$5\sigma 1\pi$		$5\sigma^{-2}$			
				$5\sigma^{-2}\pi^*$			248	$1\pi^{-1}1\pi^{-1}$			
23.2		$4\sigma^{-1}1\pi^{-1}\pi^*$	$1\pi^{-1}5\sigma^{-1}$	$4\sigma^{-1}1\pi^{-1}\pi^*$					512	$4\sigma^{-1}1\pi^{-1}$	
		$1\pi^{-2}\pi^*$		$4\sigma^{-1}5\sigma^{-1}\pi^*$						$4\sigma^{-1}1\pi^{-1}$	
		triplet									
28.4		$4\sigma^{-1}1\pi^{-1}\pi^*$	$1\pi^{-1}5\sigma^{-1}$	$4\sigma^{-2}\pi^*$		$4\sigma 5\sigma$			506	$4\sigma^{-2}$	
		$5\sigma^{-1}1\pi^{-1}\pi^*$	$4\sigma^{-1}1\pi^{-1}$	$3\sigma^{-1}$							
		triplet									
35.4		$1\pi^{-2}\pi^*$	$4\sigma^{-1}5\sigma^{-1}$								
		$4\sigma^{-1}5\sigma^{-1}\pi^*$	$4\sigma^{-1}1\pi^{-1}$								
		triplet									
39.8	247	$3\sigma^{-1}1\pi^{-1}\pi^*$	$3\sigma^{-1}2\pi^{-1}$			$3\sigma\cdots$					
		$3\sigma^{-1}$	$4\sigma^{-1}5\sigma^{-1}$								
45.5	243	$3\sigma^{-1}1\pi^{-1}\pi^*$	$3\sigma^{-1}5\sigma^{-1}$			$3\sigma\cdots$					

[a]With reference to E_f.
[b]This work CO(2×1)$p2mg$/Ni(110).
[c]Björneholm *et al.* (Refs. 25 and 26) CO/Ni(100).
[d]Wurth and co-workers (Refs. 34–36) CO/Ni(111).
[e]Ph.D. thesis, (Ref. 33) Wurth CO/Ni(111).
[f]Jennison *et al.* (Ref. 30) $Ni(CO)_4$.
[g]Umbach and Hussain (Refs. 43 and 44) CO/Ni(100).
[h]Ohno and von Niessen (Refs. 47 and 37).

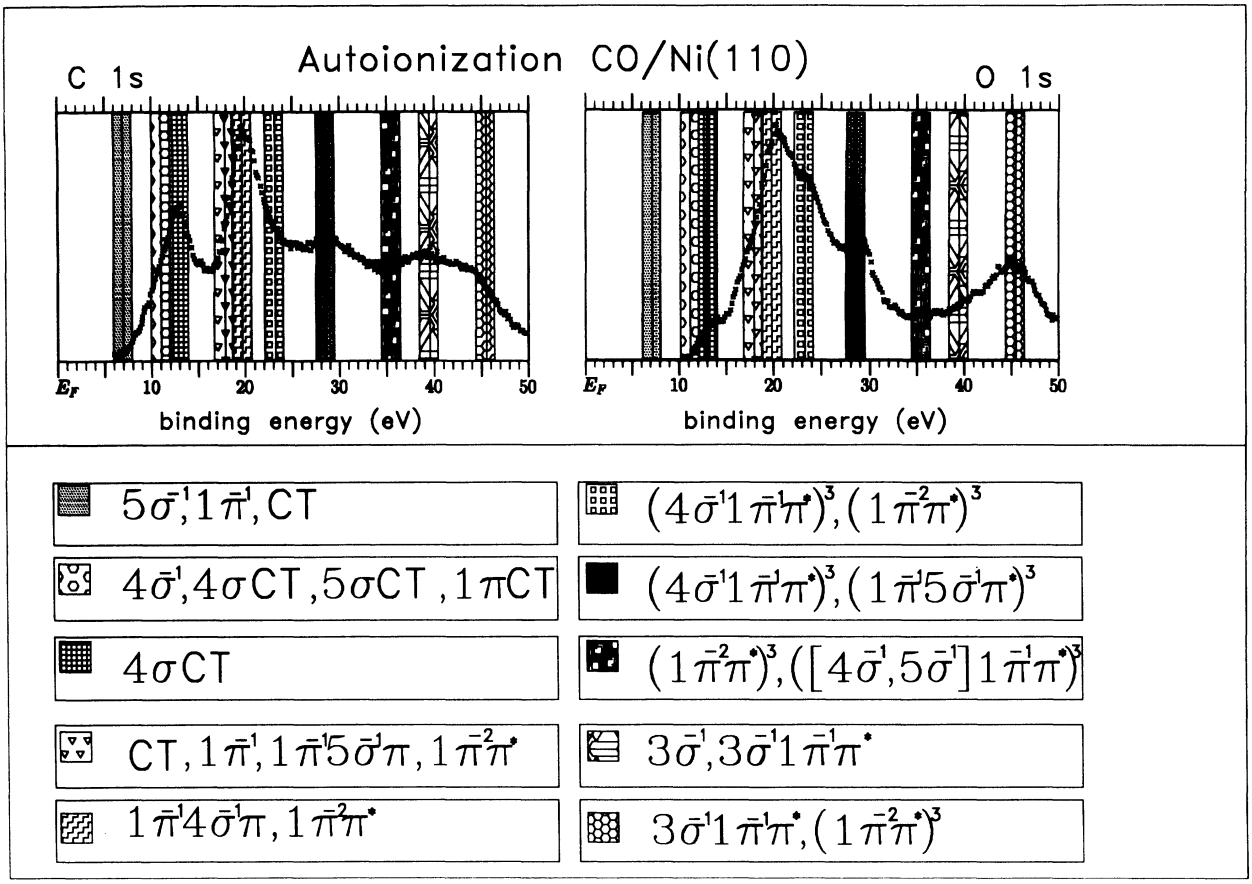

FIG. 10. Assignment of the experimental autoionization spectra. The patterns refer to particular configurations given in the boxes below the spectra.

"Bundesministerium für Forschung und Technologie" under Project No. 05 432 FAB 0. H.-J.F. thanks the Fonds der Chemischen Industrie for support. G. D. thanks the Heinrich Hertz Stiftung for support. We would also like to thank the Graduiertenkolleg "Dynamische Prozesse an Festkörperoberflächen" for financial support.

APPENDIX: ANALYSIS OF THE EXPERIMENTAL ANGULAR DEPENDENCE

The analysis of fine structures in adsorbate spectra after core-to-continuum and core-to-bound excitation is a rather difficult task. The main problems arise due to bad signal-to-noise ratios (S/N) and uncertainties of the background subtractions. In order to judge the difference spectra, it is important to realize that the clean Ni spectrum is basically represented by a flat line above 6 eV binding energy even as a function of the polar angle at the studied photon energies. Whereas the S/N ratio and the shape of the substrate spectrum can be solved experimentally, a third uncertainty still remains. It is well known that upon adsorption the amount of inelastically scattered electrons is increasing. In the present study, a

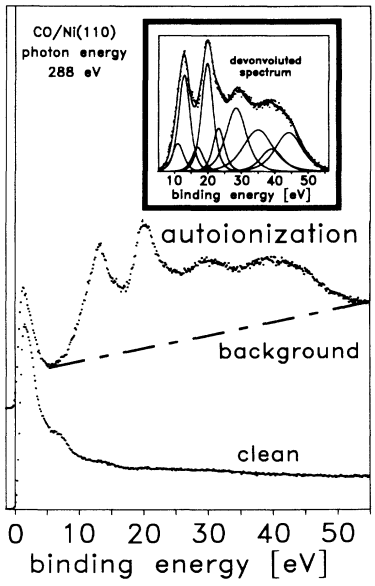

FIG. 11. Autoionization spectra after $C_{1s}\rightarrow\pi^*$ autoionization spectrum of $CO(2\times1)p2mg$/Ni(110). The chosen background is indicated. A fit with the corresponding decomposition is shown in the inset.

linear background has been subtracted from the energy interval studied. In order to study the influence of the background subtraction the energy interval has been varied. Furthermore, one has to define an angular-independent standard for a proper normalization of the individual angular-resolved spectra. It turned out that the total intensity over the energy range taken into account can be taken as an angular-independent standard. In order to study the fine structure of the autoionization spectra, we have chosen a minimum set of Lorentzian lines to deconvolute the experimental features by means of a simplex algorithm. It follows a short description of the simplex algorithm: The simplex is a geometric body defined by $(n+1)$ vectors in a n-dimensional space. The $(n+1)$th vector is the sum of the squared residuals (SSR). The algorithm proves all vectors with regard to optimizing the SSR, which means the search of the minimum SSR. To achieve this, the following mathematical operations are used: mirror, expansion, contraction, shrinking. These operations are not considered in detail here. The algorithm uses them, in given order, first for the starting simplex and then for any new simplex, until the minimum SSR is found or the program has reached a user-defined break point. The better chosen are the parameters for the starting simplex, the faster convergence of the SSR is achieved. By rule-of-thumb $4\times n^2$ iteration steps are necessary. Ten peaks have been identified in the spectra obtained after core-to-bound excitation, yielding a simplex of size 41. Usually 8000–10 000 iterations were needed to obtain convergence of the sum of the squared residuals.[75] The deconvolution of the spectra has been performed for different background subtractions in order to be able to give error bars for the individual angular dependences of the peaks.

As a prototype for the deconvoluted spectra in Fig. 11, we show an angular-resolved spectrum of the system $CO(2\times1)p2mg/Ni(110)$ after C 1*s*-to-bound excitation obtained 50° off $[1\bar{1}0]$. On the bottom of the figure, the spectrum of clean Ni is shown on a binding-energy scale referenced to the Fermi level. The top spectrum shows the raw data obtained upon adsorption of CO in the (2×1) structure. In the inset, the spectrum obtained after subtraction of a linear background is given. Furthermore, the individual Lorentzians are shown for the ten[76] peaks which have been used to deconvolute the experimental spectrum. The superposition of the individual bands is shown as a line in the spectrum and basically represents the experimental one.

[1]E. W. Plummer and W. Eberhardt, Adv. Chem. Phys. **49**, 533 (1982).

[2]N. V. Richardson and A. M. Bradshaw, in *Electron Spectroscopy Theory, Techniques and Applications*, edited by C. R. Brundle and A. D. Baker (Academic, London, 1982), Vol. 4.

[3]H.-J. Freund and M. Neumann, in *Molecular Chemisorption*, edited by S. D. Kevan (Elsevier, Amsterdam, 1992), Vol. 74.

[4]T. Koopmans, Physica **1**, 104 (1932/1933).

[5]K. Siegbahn, C. Nordling, G. Johanson, J. Heckmann, P. F. Heden, K. Hamrin, U. Gelius, T. Bergmann, Lo. O. Werme, R. Manne, and Y. Baer, *ESCA Applied to Free Molecules* (North-Holland, Amsterdam, 1969).

[6]H.-J. Freund, F. Greuter, D. Heskett, and E. W. Plummer, Phys. Rev. B **28**, 1727 (1983).

[7]T. X. Carroll and T. D. Thomas, J. Chem. Phys. **94**, 11 (1991).

[8]T. Porwol, G. Illing, H.-J. Freund, H. Kuhlenbeck, M. Neumann, S. Bernstorff, W. Braun, W. von Niessen, and C.-M. Liegener, Phys. Rev. B **41**, 10 510 (1990).

[9]P. A. Brühwiler, A. J. Maxwell, A. Nilsson, R. L. Whetten, and N. Mårtensson, Chem. Phys. Lett. **193**, 311 (1992).

[10]G. Illing, T. Porwol, I. Hemmerich, G. Dömötör, H. Kuhlenbeck, H.-J. Freund, C.-M. Liegener, and W. von Niessen, J. Electron. Spectrosc. Relat. Phenom. **51**, 149 (1990).

[11]F. P. Larkins, W. Eberhardt, I.-W. Lyo, R. Murphy, and E. W. Plummer, J. Chem. Phys. **88**, 2948 (1988).

[12]R. Dudde, Ph.D. thesis, Universität Hamburg, 1989.

[13]R. Dudde, M. L. M. Rocco, E. E. Koch, S. Bernstorff, and W. Eberhardt, J. Chem. Phys. **91**, 20 (1989).

[14]W. Eberhardt, Phys. Sci. T **17**, 28 (1987).

[15]W. Eberhardt, R. Dudde, M. L. M. Rocco, E. E. Koch, and S. Bernstorff, J. Electron. Spectrosc. Relat. Phenom. **51**, 373 (1990).

[16]C.-T. Chen, Ph.D. thesis, University of Pennsylvania, 1985.

[17]U. Becker and R. Wehlitz, Phys. Scr. **T41**, 127 (1992).

[18]D. E. Ramaker, Phys. Scr. **T41**, 77 (1992).

[19]S. Svensson and L. Karlsson, Phys. Scr. **T41**, 132 (1992).

[20]W. Eberhardt, J.-E. Rubensson, K. J. Randall, J. Feldhaus, A. L. D. Kilcoyne, A. M. Bradshaw, Z. Xu, P. D. Johnson, and Y. Ma, Phys. Scr. **T41**, 143 (1992).

[21]D. Menzel, G. Rocker, H.-P. Steinrück, D. Coulman, P. A. Heimann, W. Huber, P. Zebisch, and D. R. Lloyd, J. Chem. Phys. **96**, 1724 (1992).

[22]T. Porwol, G. Dömötör, H.-J. Freund, C.-M. Liegener, and W. von Niessen, Phys. Scr. **T41**, 197 (1992).

[23]U. Becker, R. Hölzel, H. G. Kerkhoff, B. Langer, D. Szostak, and R. Wehlitz, Phys. Rev. Lett. **56**, 1455 (1986).

[24]H.-J. Freund and C.-M. Liegener, Chem. Phys. Lett. **134**, 70 (1987).

[25]O. Björneholm, Ph.D. thesis, Uppsala University, 1992.

[26]O. Björneholm, A. Sandell, A. Nilsson, N. Mårtensson, and J. N. Andersen, Phys. Scr. **T41**, 217 (1992).

[27]A. N. de Brito, Ph.D. thesis, Uppsala University, 1991.

[28]D. M. Hanson, Adv. Chem. Phys. **77**, 1 (1990).

[29]A. P. Hitchcock, Ultramicroscopy **28**, 165 (1989).

[30]D. R. Jennison, G. D. Stucky, R. R. Rye, and J. A. Kelber, Phys. Rev. Lett. **46**, 911 (1981).

[31]S. Svensson, M. Carlsson-Göthe, L. Karlsson, A. Nilsson, N. Mårtensson, and U. Gelius, Phys. Scr. **44**, 184 (1991).

[32]W. Eberhardt, E. W. Plummer, C. T. Chen, and W. K. Ford, Aust. J. Phys. **39**, 853 (1986).

[33]W. Wurth, Ph.D. thesis, Universität München, 1987.

[34]W. Wurth, C. Schneider, R. Treichler, E. Umbach, and D. Menzel, Phys. Rev. B **35**, 7741 (1987).

[35]W. Wurth, C. Schneider, R. Treichler, D. Menzel, and E. Umbach, Phys. Rev. B **37**, 8725 (1988).

[36]W. Wurth, D. Menzel, and E. Umbach, Phys. Rev. B **45**, 3869 (1992).

[37]M. Ohno, Phys. Rev. B **45**, 3865 (1992).

[38]H. P. Steinrück, T. Pache, and W. Huber, Phys. Scr. **41**, 177 (1990).
[39]C. T. Chen, R. A. Di Dio, W. K. Ford, E. W. Plummer, and W. Eberhardt, Phys. Rev. B **32**, 8434 (1985).
[40]R. Murphy, E. W. Plummer, C. T. Chen, W. Eberhardt, and R. Carr, Phys. Rev. B **39**, 7517 (1989).
[41]W. Wurth, P. Feulner, and D. Menzel, Phys. Scr. **T41**, 213 (1992).
[42]H.-J. Freund and M. Neumann, Appl. Phys. A **47**, 3 (1988).
[43]E. Umbach and Z. Hussain, Phys. Rev. Lett. **52**, 754 (1984).
[44]E. Umbach, Comments At. Mol. Phys. **18**, 23 (1986).
[45]L. S. Cederbaum and W. Domcke, Adv. Chem. Phys. **36**, 205 (1977).
[46]L. S. Cederbaum, W. Domcke, J. Schirmer, and W. von Niessen, Adv. Chem. Phys. **65**, 115 (1986).
[47]M. Ohno and W. von Niessen, Phys. Rev. B **42**, 7370 (1990).
[48]L. S. Cederbaum, W. Domcke, J. Schirmer, and W. von Niessen, Phys. Scr. **21**, 481 (1980).
[49]D. Saddei, Ph.D. thesis, Universität Köln, 1982.
[50]D. Saddei, H.-J. Freund, and G. Hohlneicher, Surf. Sci. **95**, 527 (1980).
[51]T. Porwol, Ph.D. thesis, Ruhr-Universität Bochum, 1992.
[52]H. Siegbahn, L. Asplund, and P. Kelfve, Chem. Phys. Lett. **35**, 330 (1975).
[53]J. Cooper and R. N. Zare, in *Theoretical Physics,* edited by Sydney Geltman, Kalayara T. Mahanthappa, and Wesley E. Brittin (Gordon and Breach, New York, 1969), Vol. 11, p. 317.
[54]E. J. McGuire, Phys. Rev. **185**, 1 (1969).
[55]E. J. McGuire (unpublished).
[56]M. Abramowitz and I. A. Stegun, *Handbook of Mathematical Functions* (Dover, New York, 1972).
[57]C.-M. Liegener, Chem. Phys. Lett. **90**, 188 (1982).
[58]C.-M. Liegener, J. Chem. Phys. **79**, 2924 (1983).
[59]C.-M. Liegener, Chem. Phys. Lett. **106**, 201 (1984).
[60]C.-M. Liegener, Chem. Phys. **92**, 97 (1985).
[61]H. Ågren, A. Cesar, and C.-M. Liegener, Adv. Quant. Chem. (to be published).
[62]S. Bernstorff, W. Braun, M. Mast, W. Peatman, and T. Schroeter, Rev. Sci. Instrum. **60**, 2097 (1989).
[63]R. M. Lambert, Surf. Sci. **49**, 325 (1975).
[64]H. Kuhlenbeck, M. Neumann, and H.-J. Freund, Surf. Sci. **173**, 194 (1986).
[65]H. Kuhlenbeck, Ph.D. thesis, Universität Osnabrück, 1988.
[66]A. Nilsson and N. Mårtensson, Phys. Rev. B **40**, 10 249 (1989).
[67]A. Nilsson, Ph.D. thesis, Uppsala University, 1988.
[68]D. Saddei, H.-J. Freund, and G. Hohlneicher, Chem. Phys. Lett. **68**, 222 (1979).
[69]L. S. Cederbaum, J. Phys. B **8**, 290 (1975).
[70]J. Schirmer and L. S. Cederbaum, J. Phys. B **11**, 1889 (1978).
[71]J. Schirmer, L. S. Cederbaum, and O. Walther, Phys. Rev. A **28**, 1237 (1983).
[72]W. von Niessen, J. Schirmer, and L. S. Cedarbaum, Comput. Phys. Rep. **1**, 57 (1984).
[73]B. Bartos, H.-J. Freund, H. Kuhlenbeck, M. Neumann, H. Lindner, and K. Müller, Surf. Sci. **197**, 59 (1987).
[74]T. N. Taylor and P. J. Estrup, J. Vac. Sci. Technol. **10**, 26 (1973).
[75]I. Hemmerich, Diplomarbeit, Ruhr-Universität Bochum, 1990.
[76]One peak shows neglectable intensity at the specific azimuthal angle.